References and Notes

1. R. D. Vale, R. A. Milligan, *Science* **288**, 88 (2000).
2. A. Yildiz, M. Tomishige, R. D. Vale, P. R. Selvin, *Science* **303**, 676 (2004).
3. K. Svoboda, C. F. Schmidt, B. J. Schnapp, S. M. Block, *Nature* **365**, 721 (1993).
4. S. J. King, T. A. Schroer, *Nat. Cell Biol.* **2**, 20 (2000).
5. R. Mallik, B. C. Carter, S. A. Lex, S. J. King, S. P. Gross, *Nature* **427**, 649 (2004).
6. S. P. Gross, M. A. Welte, S. M. Block, E. F. Wieschaus, *J. Cell Biol.* **148**, 945 (2000).
7. R. Mallik, S. P. Gross, *Curr. Biol.* **14**, R971 (2004).
8. S. P. Gross *et al.*, *J. Cell Biol.* **156**, 855 (2002).
9. A. Yildiz *et al.*, *Science* **300**, 2061 (2003).
10. Materials and methods are available as supporting material on *Science* Online. For details of measurement, see (*9*). For microscopy, we used an Andor Model DV-860 BV, which is a back-illuminated camera that contains a 128 by 128 pixel sensor with 24 μm pixel size. A quarter chip is used to achieve 1 ms per frame. The incidence beam angle was tuned to get the best signal to noise. The cells were maintained at 10°C.
11. S. L. Rogers, V. I. Gelfand, *Curr. Opin. Cell Biol.* **12**, 57 (2000).
12. S. L. Rogers, G. C. Rogers, D. J. Sharp, R. D. Vale, *J. Cell Biol.* **158**, 873 (2002).
13. C. Kural *et al.*, data not shown.
14. Y. Ma, D. Shakiryanova, I. Vardya, S. V. Popov, *Curr. Biol.* **14**, 725 (2004).
15. G. Goshima, R. D. Vale, *J. Cell Biol.* **162**, 1003 (2003).
16. M. Nishiura *et al.*, *J. Biol. Chem.* **279**, 22799 (2004).
17. T. Kon, M. Nishiura, R. Ohkura, Y. Y. Toyoshima, K. Sutoh, *Biochemistry* **43**, 11266 (2004).
18. R. D. Vale, T. S. Reese, M. P. Sheetz, *Cell* **42**, 39 (1985).
19. A. J. Hunt, F. Gittes, J. Howard, *Biophys. J.* **67**, 766 (1994).
20. A. Ashkin, K. Schutze, J. M. Dziedzic, U. Euteneuer, M. Schliwa, *Nature* **348**, 346 (1990).
21. M. Lakadamyali, M. J. Rust, H. P. Babcock, X. Zhuang, *Proc. Natl. Acad. Sci. U.S.A.* **100**, 9280 (2003).
22. D. B. Hill, M. J. Plaza, K. Bonin, G. Holzwarth, *Eur. Biophys. J.* **33**, 623 (2004).
23. S. T. Brady, R. J. Lasek, R. D. Allen, *Science* **218**, 1129 (1982).
24. B. Grafstein, D. S. Forman, *Physiol. Rev.* **60**, 1167 (1980).
25. C. Kaether, P. Skehel, C. G. Dotti, *Mol. Biol. Cell* **11**, 1213 (2000).

26. We gratefully acknowledge R. Vale (University of California, San Francisco) and S. Rogers (University of North Carolina at Chapel Hill) for EGFP-EB1 and EGFP-tubulin cell lines. This work was supported by NIH grants AR44420 and GM 068625 (P.R.S.) and GM52111 (V.I.G.), an NSF grant (P.R.S.), and the U.S. Department of Energy, Division of Material Sciences (under award no. DEFG02-91ER45439), through the Frederick Seitz Materials Research Laboratory at the University of Illinois at Urbana-Champaign (P.R.S). P.R.S. also thanks J. Ackland, J. Stenehjem, and the other members of the Sharp Rehabilitation Center of San Diego for patient care, which made this science possible.

Supporting Online Material

www.sciencemag.org/cgi/content/full/1108408/DC1
Materials and Methods
Figs. S1 to S6
References

7 December 2004; accepted 30 March 2005
Published online 7 April 2005;
10.1126/science.1108408
Include this information when citing this paper.

Mechanism of Divergent Growth Factor Effects in Mesenchymal Stem Cell Differentiation

Irina Kratchmarova,[1]* Blagoy Blagoev,[1]* Mandana Haack-Sorensen,[2] Moustapha Kassem,[2] Matthias Mann[1]†

Closely related signals often lead to very different cellular outcomes. We found that the differentiation of human mesenchymal stem cells into bone-forming cells is stimulated by epidermal growth factor (EGF) but not platelet-derived growth factor (PDGF). We used mass spectrometry–based proteomics to comprehensively compare proteins that were tyrosine phosphorylated in response to EGF and PDGF and their associated partners. More than 90% of these signaling proteins were used by both ligands, whereas the phosphatidylinositol 3-kinase (PI3K) pathway was exclusively activated by PDGF, implicating it as a possible control point. Indeed, chemical inhibition of PI3K in PDGF-stimulated cells removed the differential effect of the two growth factors, bestowing full differentiation effect onto PDGF. Thus, quantitative proteomics can directly compare entire signaling networks and discover critical differences capable of changing cell fate.

Receptor tyrosine kinases (RTKs) regulate cellular processes ranging from cell growth and proliferation to survival and differentiation. After binding of their cognate ligands, these receptors undergo autophosphorylation on multiple tyrosine residues and become a platform for binding and consequent tyrosine phosphorylation of various signaling molecules, thus triggering multiple signaling cascades (*1*–*3*). To transmit the signal across the entire cell, various RTKs often activate universal signaling pathways. Nevertheless, distinct and even opposing biological effects of these receptors can arise.

Human mesenchymal stem cells (hMSC) are nonhematopoietic cells that reside within the bone marrow stroma. These cells are multipotent and serve as precursors for various mesoderm-type cells (*4*, *5*). Thus, hMSC have great clinical potential in tissue regeneration and engineering protocols (*6*). In cell culture, they can give rise to osteoblasts, adipocytes, and chondrocytes through processes largely controlled by various growth factors (*7*, *8*).

To study the effects of growth factors on hMSC, we first tested the effects of EGF, PDGF, fibroblast growth factor (FGF), and nerve growth factor (NGF) on cellular responses. Using immunoprecipitation and Western blotting with antibodies to phosphotyrosine, we observed that EGF and PDGF elicited the strongest responses (*9*) and that they induced phosphorylation of common and distinct subsets of proteins (Fig. 1A). Because one of the main characteristics of hMSC is their ability to differentiate to osteoblasts, we explored the possibility that these growth factors affect osteogenic conversion. The induction of the osteoblast differentiation pathway is indicated by increased alkaline phosphatase in the early stages (day 2 to 4), and in vitro mineralization is a marker for mature osteoblasts

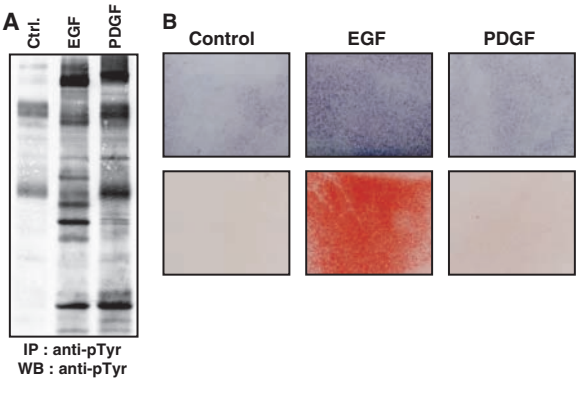

Fig. 1. Response of hMSC to EGF and PDGF stimulation. (**A**) Anti-phosphotyrosine (anti-pTyr) Western blotting (WB) of non-stimulated (Ctrl.) or EGF- or PDGF-stimulated hMSC, after immunoprecipitation (IP) with anti-pTyr. (**B**) Effects of EGF and PDGF on hMSC osteoblast differentiation. (Top) Alkaline phosphatase activity at day 3 of differentiation, visualized by in situ staining. (Bottom) Extracellular matrix in vitro mineralization after 9 days; staining with Alizarin Red S dye.

[1]Center for Experimental BioInformatics (CEBI), Department of Biochemistry and Molecular Biology, University of Southern Denmark, Campusvej 55, DK-5230 Odense M, Denmark. [2]Department of Endocrinology, Odense University Hospital, DK-5000 Odense C, Denmark.

*These authors contributed equally to this work.
†To whom correspondence should be addressed. E-mail: mann@bmb.sdu.dk

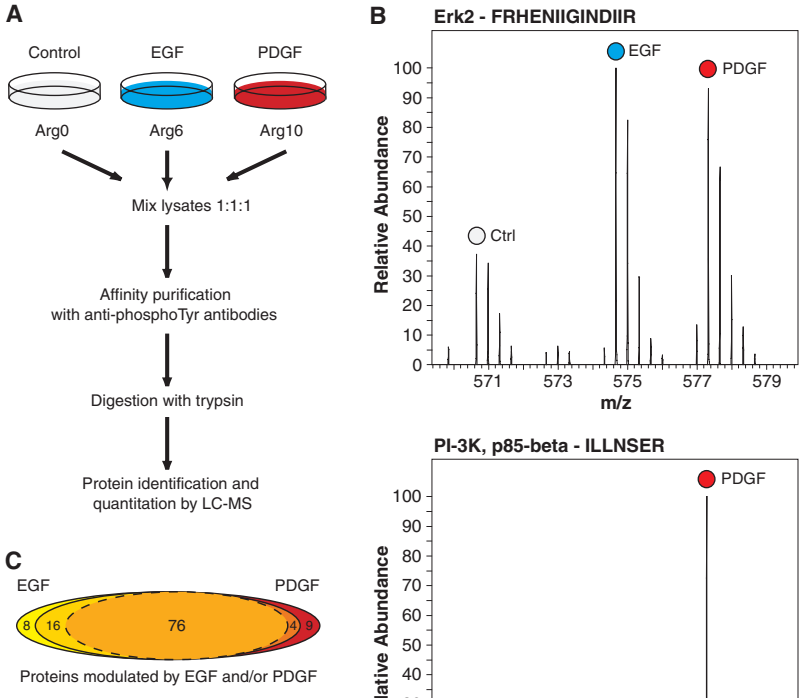

Fig. 2. Determination of EGF and PDGF phosphoprotein complexes in hMSC. (**A**) Strategy for identification and quantitative comparison of the global EGF and PDGF signaling networks. Three populations of hMSC are metabolically encoded with either normal arginine (Arg^0), or versions which are 6 daltons heavier (Arg^6) or 10 daltons heavier (Arg^{10}). After treatment with growth factors and immunoprecipitation with antibodies to pTyr, precipitated complexes are digested with trypsin and analyzed by mass spectrometry. (**B**) The degree of activation by EGF and PDGF is reflected in the ratio of the Arg^6 and Arg^{10}-containing peptides, respectively, over the Arg^0 peptides. The peptide FRHENIIGINDIIR of Erk2 (top) shows equal response of Erk2 to both growth factors, whereas the peptide ILLNSER of p85-β subunit (bottom) reveals PDGF-specific stimulation of PI3K. (**C**) Distribution of proteins involved in EGF and PDGF signaling networks. The two ellipses with solid lines contain all proteins involved in EGF (left) and PDGF (right) signaling. The overlapping area comprises the molecules common for the two signaling networks with the inner punctuated ellipse representing the proteins that were stimulated at comparable levels (within a factor of 3).

(day 9 to 12) (*10*, *11*). The addition of EGF during the course of differentiation resulted in increased activity of alkaline phosphatase (Fig. 1B, upper panel) and enhanced formation of mineralization nodules (Fig. 1B, lower panel), whereas PDGF had no effect, despite its ability to induce tyrosine phosphorylation.

To discover critical differences in the signaling mechanisms of EGF and PDGF that led to the differential effects on osteoblast differentiation of hMSC, we sought to identify and directly compare the signaling proteins regulated by tyrosine phosphorylation in response to these growth factors by mass spectrometry (MS)–based proteomics (*12*–*16*). We used stable isotope labeling by amino acids in cell culture (SILAC) (*17*), a quantitative proteomic strategy that metabolically labels the entire proteome, making it distinguishable by MS analysis. Three populations of hMSC were grown in medium containing distinct forms of arginine—either the normal $^{12}C_6$, $^{14}N_4$ version (Arg^0), or the isotopic variants $^{13}C_6$, $^{14}N_4$ (Arg^6) or $^{13}C_6$, $^{15}N_4$ (Arg^{10})—until full incorporation of the labeled amino acid was achieved. Arg^0 cells were left untreated and served as a control, Arg^6 cells were exposed to EGF, and Arg^{10} cells were exposed to PDGF (Fig. 2A). The combined cellular lysates from the three states were incubated with antibodies to phosphotyrosine. The precipitated complexes were resolved on one-dimensional SDS–polyacrylamide gel electrophoresis and proteolytically digested. The resulting peptide mixture was analyzed by liquid chromatography–tandem MS (LC-MS/MS). Tyrosine-phosphorylated proteins and proteins associated with them are efficiently isolated in this way. Arginine-containing peptides occur as triplets in the mass spectra and

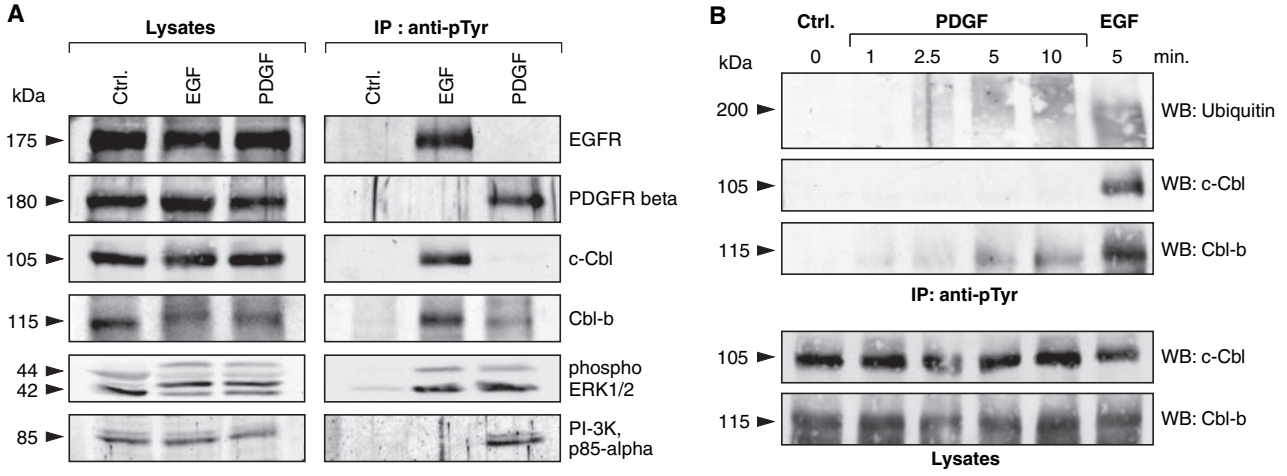

Fig. 3. Western blot (WB) analysis of selected proteins regulated by EGF and PDGF. (**A**) After 5 min stimulation with EGF or PDGF, hMSC were lysed and immunoprecipitated (IP) with antibodies to pTyr followed by Western blotting for indicated proteins. In the case of Erk1 and Erk2, lysates were directly probed with phospho-Erk1/2–specific antibody. Separate immunoblotting on the lysates is shown to serve as loading control. (**B**) Time course of PDGF receptor ubiquitination, c-Cbl and Cbl-b activation. hMSC were stimulated with PDGF for the indicated time points and 5 min stimulation with EGF was used for comparison. After anti-pTyr immunoprecipitation, Western blotting with the corresponding antibodies was used to visualize receptor ubiquitination and Cbl activation. In the lower panel, the cellular lysates were directly probed with antibodies against c-Cbl and Cbl-b to serve as loading control.

the intensity ratios of the Arg^6 and Arg^{10} to the control Arg^0 peptide directly reflect the degree of tyrosine phosphorylation of the corresponding protein or its association with other tyrosine-phosphorylated proteins as a result of the treatment with EGF and PDGF, respectively (Fig. 2B) (*15*, *16*).

We performed two independent experiments and in total identified 113 proteins with 1.5-fold or higher change in abundance in antiphosphotyrosine immunoprecipitates as a consequence of the treatment by at least one of the growth factors (Table 1). Each of these proteins was identified with at least two unique peptides, at high mass accuracy and with manual verification, ensuring no false-positive identifications in this data set. In the first experiment, we used 5×10^7 cells per condition and a quadrupole time-of-flight (QSTAR) mass spectrometer. From all 150 quantified proteins, we distinguished 79 proteins (table S1) whose abundance in the immunoprecipitates was altered after growth factor treatment. In the second experiment, we used 1.1×10^8 cells and a linear ion trap Fourier Transform (LTQ-FT) mass spectrometer and identified 106 modulated proteins from a total of 282 quantified proteins. The LTQ-FT analysis quantified all but seven of the proteins in the QSTAR data set and added another 34 because of its higher sensitivity, sequencing speed, and ability to handle larger sample amounts (table S1).

To verify the MS data set, we compared the proteomic results with a series of independent immunoblotting experiments with antibodies to 20 representative proteins regulated by EGF or PDGF. Although Western blotting is not quantitative per se, complete concordance was observed between immunoblotting and quantitative proteomic results (Table 1 and fig. S1).

After verifying the set of regulated proteins, we estimated the biological variability in the magnitude of the response of individual proteins within the measured sets. Quantitative proteomics indicated that about 90% of the proteins showed similar changes in abundance between the two large-scale experiments (within a factor of 1.3 of their average fold change; table S1 and fig. S2). For very high fold changes, agreement was also good; however, in some cases normalization to a low basal signal led to larger variation.

Many signaling molecules were found at similar amounts in the tyrosine-phosphorylated complexes of EGF- and PDGF-stimulated cells, whereas some proteins showed specific activation by one or the other of the growth factors. On the basis of the observed fold change in abundances, we categorized all 113 proteins (Table 1). Both EGF and PDGF activate a range of widely shared signaling pathways. Examples include the mitogen-activated protein kinase (MAPK) cascades and signal attenuation through receptor ubiquitination followed by endocytic removal from the cell surface (*1*, *18*). Therefore, it is not surprising that a large number of the molecules in Table 1 showed increased presence in phosphotyrosine-containing complexes from cells treated with either ligand. Less than 10% of the EGF- or PDGF-modulated proteins were unique to each growth factor (Fig. 2C).

Only five proteins showed decreased abundance in tyrosine-phosphorylated complexes of growth factor–treated cells, including a protein tyrosine kinase 9 (PTK9)–like kinase that had not previously been linked to regulation by EGF or PDGF receptors. This group contains breast cancer anti-estrogen resistance 1 protein (BCAR1), which is the human homolog of the focal adhesion docking protein p130Cas, and BCAR3, which is the human homolog of AND-34, a protein that binds to BCAR1 (*19*). The amounts of BCAR1 and BCAR3 in the immunoprecipitates were decreased in response to EGF but increased in response to PDGF (Table 1 and fig. S1), suggesting diverse roles downstream of these growth factors.

We further divided proteins based on the magnitude of their change in abundance in phosphotyrosine-containing complexes in cells treated with EGF or PDGF. We classified a protein as considerably more responsive to one ligand if its change in abundance was at least three times greater than that from cells treated with the other ligand. Several interesting observations became apparent through this categorization. For example, activated EGF and PDGF receptors appear to be preferentially attenuated by different mechanisms. Major proteins involved in the removal of the receptors from the cell membrane and its subsequent endocytosis were all much more abundant in immune complexes from EGF-treated cells, consistent with the well-known pathway involving Eps15 interacting protein (Epsin), Casitas B-lineage lymphoma proto-oncogene (Cbl), EGFR substrate 15 (Eps15), hepatocyte growth factor–regulated tyrosine kinase substrate (Hrs), signal-transducing adaptor molecule (STAM), and STAM2 (*18*, *20*) (Table 1 and fig. S1). Activated PDGF receptors, on the other hand, appear to undergo a different (or possibly delayed) endocytic pathway, mostly dependent on target of Myb1 (TOM1) and Toll-interacting protein (TOLLIP). These two proteins function in endosomal trafficking (*21*) but had not been associated with RTKs. The tyrosine phosphatase Shp-2 was also more responsive to PDGF, which could indicate faster dephosphorylation of members of the PDGF phosphoproteome (Table 1 and fig. S1).

Src homologous and collagen (Shc) and son of sevenless protein homolog 1 (Sos1)

Table 1. Proteins with altered amounts in phosphotyrosine-containing complexes after treatment of hMSC with EGF or PDGF. Proteins are categorized on the basis of their fold change (ratio) in abundances. Ratios are averages of two large-scale experiments (table S1) (*33*).

Protein name	Ratio in EGF	Ratio in PDGF
Specific proteins for EGF		
EGFR	33.7	1.09
ErbB2	12.3	1.06
c-Cbl	75	1.05
DOC-2	33.3	1.08
Acid phosphatase 1	1.62	0.87
Ribonuclease inhibitor	2.20	1.10
CYLD	21.7	1.00
KIAA2002	2.85	1.03
Specific proteins for PDGF		
PDGFR α	1.48	42
PDGFR β	0.90	56
PI-3K, p85-α	1.07	3.62
PI-3K, p85-β	0.96	6.2
PI-3K, p110-α	1.07	7.2
PI-3K, p110-β	0.91	2.20
PI-3K, p110-δ	0.86	5.9
Fyn	0.93	3.5
Protocadherin 43	1.07	14.1
Proteins with increased abundance in both EGF and PDGF		
Considerably higher in EGF		
Eps15	33.6	8.2
Cbl-b	9.5	2.01
Hrs	23.6	4.95
Epsin 2a	25.2	4.22
STAM	19.7	4.13
STAM2	27.4	5.8
Sts-1	10.9	1.93
Shc	5.7	1.49
Sos 1	7.93	1.73
SHIP2	9.0	1.73
p62Dok	17.7	2.35
p120 Catenin	7.50	1.78
CED12A	5.7	1.15
BICD2	5.69	1.12
NSAP1/hnRNP Q	4.07	1.23
EIF-2A	11.9	1.53
Considerably higher in PDGF		
Shp-2	3.74	18.0
RasGAP	2.48	16.5
TOM1	3.42	10.4
TOLLIP	2.57	7.0
Similar levels in EGF and PDGF		
Ubiquitin	11.8	17.3
TOM1L2	10.9	18.2
TSG101	4.98	8.7
Grb2	2.33	1.59
Sos 2	4.88	2.22
Erk1	2.76	2.05
Erk2	2.73	2.29
p38 Map kinase	2.77	1.92
ACK1	2.18	2.23
PLC-γ	10.7	15.7
Hypothetical- PLC-γ like	8.7	12.9
Gab1	3.11	2.91
Ras GAP-like, IQGAP 1	1.53	2.01
Vav-2	2.79	1.43
Rho GEF 6	1.48	2.40
Rho GEF 7	2.54	3.40
ARF GAP, GIT2	1.73	3.62

Table 1 continued.

Protein name	Ratio in EGF	Ratio in PDGF
Rab-6	1.61	1.46
NCK1	1.71	2.38
PDCD6-interacting protein	10.2	6.5
PDCD6IP	9.4	4.4
HECT domain LASU1	2.35	3.31
PP2A, subunit A	1.67	1.60
ApolipoproteinE receptor	2.16	2.48
AXL	1.94	1.79
Eck/EphA2	1.34	2.46
DDR2	2.57	2.23
Caveolin	1.70	1.49
PICALM	5.45	5.26
Vps28 homolog	2.83	2.26
Ymer	27.0	10.9
ANKRD13 protein	14.9	15.6
WWdomain binding protein2	4.26	5.79
FAK1	1.32	2.35
Vinculin	1.39	1.72
Paxillin	1.63	2.38
Ezrin	3.35	2.33
Catenin, β 1	2.36	1.17
Tight junction protein ZO-1	2.62	1.44
Tight junction protein ZO-2	2.54	1.48
Sorcin	4.96	2.27
Alpha-actinin 1	1.73	1.35
Alpha actinin 4	1.61	1.19
Tubulin α	2.02	1.11
ARP2	1.69	2.30
ARP3	1.53	2.06
ARP2/3, subunit 1A	1.37	1.84
ARP2/3, subunit 1B	1.77	2.21
ARP2/3, subunit 2	1.58	2.13
ARP2/3, subunit 3	1.56	2.05
ARP2/3, subunit 4	1.57	2.07
ARP2/3, subunit 5	1.60	2.10
Similar to ARP2/3, sub 5	1.71	2.05
Flightless I homolog	1.38	1.79
Gelsolin	1.37	1.87
hnRNP K	2.18	1.68
Major vault protein	1.42	1.81
PTRF	2.20	1.29
EIF-4H	1.76	1.28
NPAS 1	1.84	2.27
FAT gene product	3.24	1.48
TAK1-binding protein 1	5.70	2.22
TRK-fused gene	4.18	1.95
14-3-3 ζ/δ	1.50	1.45
14-3-3 τ	1.63	1.49
SNX3	2.45	2.94
SNX12	3.46	2.94
Annexin I	2.21	1.65
Annexin VI	1.33	1.60
Annexin VII	9.9	3.80
Annexin XI	10.9	4.0
Proteins with decreased abundance in both EGF and PDGF		
Cytochrome c	0.26	0.27
NDP kinase B	0.36	0.52
PTK9-like protein	0.61	0.59
Decreased in EGF but increased in PDGF		
BCAR1	0.44	1.64
BCAR3	0.42	1.78

had accumulated to greater extent in immunoprecipitates from EGF-stimulated cells, and growth factor receptor-bound protein 2 (Grb2) and Sos2 were also more abundant compared with immunoprecipitates from PDGF-stimulated cells. The critical role of the canonical Shc, Grb2, Sos pathway in MAPK activation is well established (*1*), yet we observed very similar amounts of phosphorylated extracellular signal–regulated kinase (Erk1) and Erk2 after exposure of cells to EGF or PDGF (Table 1 and Fig. 3A). This may imply existence of additional means of MAPK stimulation by PDGF in hMSC or of stronger negative-feedback regulation of the cascade in the case of EGF.

Surprisingly few signaling factors were uniquely affected only by one of the two ligands: only eight for EGF and nine for PDGF. This group includes the activated receptors: EGFR and ErbB2 for EGF and PDGFR α and PDGFR β for PDGF. We discovered a previously unrecognized kinase, KIAA clone 2002, specific to EGF but not PDGF signaling. A major difference in the activation profiles by the two growth factors is related to the ubiquitination of the EGF and PDGF receptors. c-Cbl is thought to be the main E3 ubiquitin ligase responsible for the ubiqitination of both types of receptors (*22*, *23*). We did find more than a 70-fold increase of c-Cbl in the phosphotyrosine immunoprecipitates from cells treated with EGF. In PDGF-stimulated cells, however, no increase in the amount of immunoprecipitated c-Cbl was detected (Table 1 and Fig. 3A), suggesting that c-Cbl does not associate with PDGF receptor. Although the abundance of Cbl-b, a related E3 ubiquitin ligase, in the immunoprecipitates was elevated as a result of the treatment with either of the growth factors, much higher fold increase was observed after EGF stimulation (Table 1 and Fig. 3A). However, the ubiquitination of the receptors after 5 min of stimulation (quantified from arginine-containing ubiquitin peptides derived from the same gel bands as the receptors) was similar or even slightly higher for the PDGF receptors (Table 1 and fig. S1). A possible explanation could be that within 5 min c-Cbl was already dephosphorylated and dissociated from PDGFR or that Cbl-b is the only E3 ubiquitin ligase downstream of PDGF receptors. We stimulated hMSC with PDGF for 1, 2.5, 5, or 10 min and monitored PDGFR ubiquitination and the levels of c-Cbl and Cbl-b activation. c-Cbl was not associated with PDGFR at any time up to 10 min, whereas receptor ubiquitination correlated with increasing presence of Cbl-b in phosphotyrosine-containing complexes (Fig. 3B). Similar results were observed in human embryonic kidney 293T cells by cotransfecting PDGFR along with c-Cbl or Cbl-b (fig. S3), supporting our finding that at least in some cell types Cbl-b is the Cbl ubiquitin ligase downstream of PDGF receptors.

A notable difference in the signaling pathways activated by the two growth factors in hMSC also stood out. Accumulation of components of the PI3K pathway was detected only after cells were treated with PDGF but not with EGF. However, both ligands caused accumulation of similar levels of Erk1, Erk2, and p38 (Table 1, Fig. 3A, and fig. S1). Moreover, we identified as specific for PDGF all of the regulatory (p85 α and β) and catalytic subunits (p110 α, β, and δ) of the PI3K; the amounts of these subunits increased on average fivefold. However, the highest ratio of any subunit upon EGF stimulation was 1.07, which is not a significant change. PI3K phosphorylates inositol lipids at the 3′ position of the inositol ring, leading to activation of Akt among other important signaling events. In osteoblasts, PI3K regulates migration and survival (*24*, *25*), but its role in the differentiation processes remains unclear and somewhat controversial (*26*, *27*).

As described above (Fig. 1B), treatment of hMSC with EGF resulted in stimulation of osteoblast differentiation, whereas PDGF did not have any effect. Because PI3K was the obvious difference between the signaling pathways induced by PDGF compared with those induced by EGF, we investigated whether the PI3K cascade could account for that divergence. We used a chemical biology strategy to block both common and specific branches of EGF- and PDGF-induced pathways. First, we applied a specific MAPK inhibitor, U0126 (*28*), to examine the role of MAPKs in osteoblast differentiation. U0126 (10 μM) completely eliminated phosphorylation, and thus activation, of Erk1 and Erk2 (fig. S4A). The addition of U0126, either to control cells or cells treated with the growth factors, also completely abolished the differentiation of hMSC to osteoblasts, verifying the critical importance of MAPK for the osteoblast conversion process (Fig. 4, A and B) (*10*, *29*). A similar effect on osteoblast differentiation was observed when hMSC were treated with p38 inhibitor (SB203580, 10 μM), suggesting that in these cells p38 activation is needed for osteoblast conversion (fig. S5).

Treatment of cells with the PI3K-specific inhibitor Wortmannin (75 nM) (*30*) inhibited PDGF-induced activation of the PI3K cascade, as measured by phosphorylation of a downstream effector Akt (fig. S4B) (*31*). Inhibition of PI3K by Wortmannin in PDGF-treated cells resulted in enhanced osteoblast differentiation compared with that of cells treated with PDGF alone. Alkaline phosphatase activity (Fig. 4A) and in vitro mineralization (Fig. 4B) in these cultures were substantially enhanced, completely mimicking the levels of stimulation observed after treatment with EGF. Furthermore, we implanted differentially treated hMSC into immunodeficient mice and determined new-

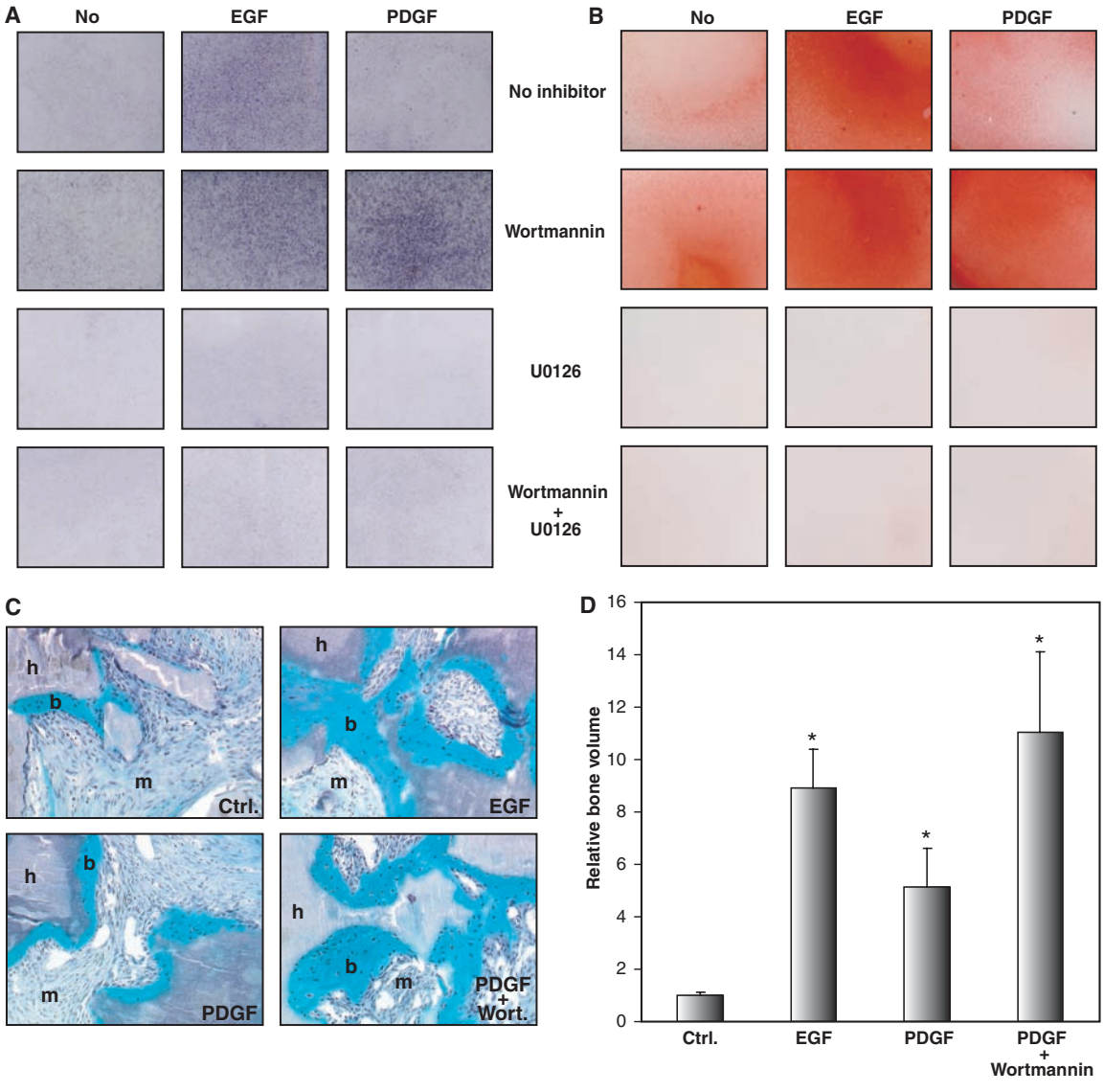

Fig. 4. Effects of PI3K and MAPK inhibitors on osteoblast differentiation and in vivo bone formation. Differentiation of hMSC to osteoblasts was carried out in the presence of EGF or PDGF. Where indicated, Wortmannin (75 nM) and U0126 (10 μM) were added in the media either alone or in combination. (**A**) Alkaline phosphatase in situ staining was performed 3 days after treatment. (**B**) Extracellular matrix mineralization at day 9 was visualized by Alizarin Red S staining. (**C**) In vivo bone formation of hMSC differentially treated for 4 days and recovered from mice after 5 weeks. Sections of implants (magnification 100×) were stained with Goldner's trichrome; bone (b), marrow (m), hydroxyapatite/tricalcium phosphate (h). Bone volume was quantified as percent of total implant volume and presented relative to control. (**D**) Three implants were used for each condition. Values are mean ± SEM. The bone volume was calculated from three distinct areas of each implant. Data were analyzed by one-way analysis of variance followed by Student-Newman-Keuls multiple range test. *P* values for bars marked with asterisks: control to EGF and control to PDGF+Wortmannin, $P < 0.001$; EGF to PDGF, $P < 0.03$; PDGF to PDGF+Wortmannin, $P < 0.01$.

ly formed bone in the transplants (Fig. 4, C and D) (*32*). In accordance with the results from cell culture differentiation, EGF-treated cells displayed enhanced bone formation in vivo. Although PDGF-treated cells also produced larger bone volume compared with that of the control, the combined treatment with PI3K inhibitor resulted in substantially increased bone formation to a level even higher than those induced by EGF (Fig. 4D). Thus, the PI3K pathway is indeed a critical control point that determines the differences of EGF and PDGF in stimulating hMSC differentiation.

We used global, quantitative phosphoproteomics to elucidate differences in closely related phosphoproteomes and to connect them with cell fate decisions. Mathematical models in systems biology have concentrated on MAPK signaling and it is hypothesized that strength and frequency of activation at this level influence cell fate. Our results demonstrated that, at least in some cases, decisions can be made by preferentially activating a small subset of the signaling network, beginning at the level of plasma membrane–associated signaling. Extensions of this work could be directed at following changes through the Ser-Thr phosphoproteome, especially related to transcription factors and transcriptional coregulators. This type of analysis provides a mechanistic "missing link" between different stimuli and resulting changes in transcription as measured by microarrays. It is possible, with a combination of proteomics and chemical biology, to discover pathways that influence cell fate. Such approaches could be beneficial for applications of stem cells to direct stem cell differentiation to clinical need more precisely.

References and Notes

1. J. Schlessinger, *Cell* **103**, 211 (2000).
2. T. Pawson, P. Nash, *Science* **300**, 445 (2003).
3. P. Blume-Jensen, T. Hunter, *Nature* **411**, 355 (2001).
4. M. F. Pittenger *et al.*, *Science* **284**, 143 (1999).
5. K. W. Liechty *et al.*, *Nat. Med.* **6**, 1282 (2000).
6. P. Bianco, P. G. Robey, *Nature* **414**, 118 (2001).
7. M. Reyes, C. M. Verfaillie, *Ann. N. Y. Acad. Sci.* **938**, 231 (2001).
8. J. L. Simonsen *et al.*, *Nat. Biotechnol.* **20**, 592 (2002).
9. I. Kratchmarova, B. Blagoev, M. Mann, data not shown.
10. R. K. Jaiswal *et al.*, *J. Biol. Chem.* **275**, 9645 (2000).
11. H. Qi *et al.*, *Proc. Natl. Acad. Sci. U.S.A.* **100**, 3305 (2003).
12. R. Aebersold, M. Mann, *Nature* **422**, 198 (2003).
13. W. X. Schulze, M. Mann, *J. Biol. Chem.* **279**, 10756 (2004).
14. J. A. Ranish *et al.*, *Nat. Genet.* **33**, 349 (2003).
15. B. Blagoev *et al.*, *Nat. Biotechnol.* **21**, 315 (2003).
16. B. Blagoev, S. E. Ong, I. Kratchmarova, M. Mann, *Nat. Biotechnol.* **22**, 1139 (2004).
17. S. E. Ong *et al.*, *Mol. Cell. Proteomics* **1**, 376 (2002).
18. I. Szymkiewicz, O. Shupliakov, I. Dikic, *Biochem. J.* **383**, 1 (2004).
19. R. B. Riggins, L. A. Quilliam, A. H. Bouton, *J. Biol. Chem.* **278**, 28264 (2003).

20. M. D. Marmor, Y. Yarden, *Oncogene* **23**, 2057 (2004).
21. Y. Katoh *et al.*, *J. Biol. Chem.* **279**, 24435 (2004).
22. C. B. Thien, W. Y. Langdon, *Nat. Rev. Mol. Cell Biol.* **2**, 294 (2001).
23. K. Haglund *et al.*, *Nat. Cell Biol.* **5**, 461 (2003).
24. F. Debiais *et al.*, *Exp. Cell Res.* **297**, 235 (2004).
25. R. Fukuyama *et al.*, *Biochem. Biophys. Res. Commun.* **315**, 636 (2004).
26. N. Ghosh-Choudhury *et al.*, *J. Biol. Chem.* **277**, 33361 (2002).
27. F. Vinals, T. Lopez-Rovira, J. L. Rosa, F. Ventura, *FEBS Lett.* **510**, 99 (2002).
28. M. F. Favata *et al.*, *J. Biol. Chem.* **273**, 18623 (1998).
29. C. F. Lai *et al.*, *J. Biol. Chem.* **276**, 14443 (2001).
30. T. Okada, L. Sakuma, Y. Fukui, O. Hazeki, M. Ui, *J. Biol. Chem.* **269**, 3563 (1994).
31. T. F. Franke *et al.*, *Cell* **81**, 727 (1995).
32. B. M. Abdallah *et al.*, *Biochem. Biophys. Res. Commun.* **326**, 527 (2005).
33. Materials and methods are available as supporting material on *Science* Online.
34. We thank all members of our laboratory for help and fruitful discussions, especially C. de Hoog for critical reading of the manuscript, J. V. Olsen for help with the LTQ-FT and statistical analysis and S.-E. Ong for help with data analysis. We thank I. Dikic for the kind gift of hemagglutinin-tagged constructs of c-Cbl and Cbl-b. Work in CEBI is supported by a grant by the Danish National Research foundation. This work was also supported by "Interaction Proteome," a 6th Framework program of the European Commission.

Supporting Online Material
www.sciencemag.org/cgi/content/full/308/5727/1472/DC1
Materials and Methods
Figs. S1 to S5
Table S1
References

17 November 2004; accepted 7 April 2005
10.1126/science.1107627

The Structure of Interleukin-2 Complexed with Its Alpha Receptor

Mathias Rickert,* Xinquan Wang,* Martin J. Boulanger, Natalia Goriatcheva, K. Christopher Garcia†

Interleukin-2 (IL-2) is an immunoregulatory cytokine that binds sequentially to the alpha (IL-2Rα), beta (IL-2Rβ), and common gamma chain (γ_c) receptor subunits. Here we present the 2.8 angstrom crystal structure of a complex between human IL-2 and IL-2Rα, which interact in a docking mode distinct from that of other cytokine receptor complexes. IL-2Rα is composed of strand-swapped "sushi-like" domains, unlike the classical cytokine receptor fold. As a result of this domain swap, IL-2Rα uses a composite surface to dock into a groove on IL-2 that also serves as a binding site for antagonist drugs. With this complex, we now have representative structures for each class of hematopoietic cytokine receptor–docking modules.

Interleukin-2 (IL-2), which is one of the first cytokines identified and a member of the four-helix bundle cytokine superfamily, acts at the heart of the immune response (*1*). IL-2 and its alpha receptor, IL-2Rα, are expressed by T cells after the activation of T cell receptors by peptide–major histocompatibility complexes. The subsequent autocrine interaction of IL-2 with its receptors leads to the stimulation of signal transduction pathways resulting in T cell, B cell, and natural killer (NK) cell proliferation and clonal expansion (*2*).

The pleiotropic biological activities of IL-2 are mediated by three cell surface receptors: the IL-2Rα chain; the IL-2Rβ chain; and the common gamma chain (γ_c), which is also a receptor for IL-4, IL-7, IL-9, IL-15, and IL-21 (*3*). These cell surface receptors form a complex that signals through the intracellular activation of the Janus tyrosine kinase 3 (Jak3) and the signal transducer and activator of transcription 5 (STAT5) (*4*). The IL-2Rα chain, originally identified as the Tac antigen (CD25) (*5*–*7*), is enigmatic in that it lacks signature features of the cytokine receptor superfamily (*8*). IL-2Rβ (p75) and the γ_c are both members of the hematopoietic growth factor receptor family, containing the signature cytokine-binding homology region (CHR), which is composed of two fibronectin type-III (FN-III) repeats (*2*, *8*).

Biochemical studies show that the assembly of the IL-2 receptor complex is initiated by the interaction of IL-2 with IL-2Rα, followed by sequential recruitment of IL-2Rβ and γ_c (*9*, *10*). IL-2Rα alone is the "low-affinity" receptor (dissociation constant $K_d \sim 10$ nM). When expressed together, IL-2Rα and IL-2Rβ form the pseudo–high-affinity receptor ($K_d \sim 30$ pM). Finally, the IL-2Rα$\beta\gamma_c$ complex forms the high-affinity receptor ($K_d \sim 10$ pM) that is the signaling complex found on activated T cells (*2*). The IL-2Rβ and γ_c binding sites on IL-2 have been mapped to locations analogous to the site I and site II cytokine-binding sites originally established in the human growth hormone (hGH) system (*11*). However, based on sequence analysis and mutagenesis studies, IL-2Rα is predicted to differ from other cytokine receptors in both its structure and its mode of interaction with IL-2 (*12*).

IL-2Rα is a target for therapeutic modulation because it is not expressed on resting T and B cells but is continuously expressed by the abnormal T cells of patients with forms of leukemia, autoimmunity, and organ transplant rejection (*13*, *14*). An antagonistic monoclonal antibody to IL-2Rα (anti-Tac) (Daclizumab) is effective in preventing the rejection of organ transplants (*15*). Small-molecule inhibitors of IL-2Rα have also been developed (*16*, *17*). IL-2 (Proleukin) itself is used to augment immune system function and has efficacy in treating metastatic renal carcinoma and melanoma (*18*). However, there is severe dose-limiting toxicity that is largely attributed to activation of the $\beta\gamma_c$ form of the receptor on NK cells (*18*). Currently, no structural information exists for any of the IL-2 receptors, and this information could assist in the design of improved therapeutics. Here we present a crystal structure at 2.8 Å resolution of human IL-2 in complex with the extracellular domain of IL-2Rα (*19*).

In the complex structure, the IL-2Rα ectodomain resembles an arm bent ~90° at the elbow between the N- and C-terminal domains (D1 and D2, respectively), engaging IL-2 along the length of the underside of D1 (Fig. 1, A and B). The IL-2 binding surface comprises helix A′, helix B′, and part of the AB loop. The long axes of the IL-2Rα β sheets are aligned parallel with the helical axes of the cytokine. This differs from the typical cytokine receptor interaction. For example, in the complex of hGH with its receptor (hGH-R), the CHR module of hGH-R, composed of two β-sandwich FN-III domains, forms a considerably larger, but similar, bent arm–like structure (Fig. 1B) (*20*). However, the protruding elbow region of hGH-R exposes loops that bind to the sides of the hGH four-helix bundle (*20*) (Fig. 1B). Although substantially different, the closest similarity can be found in the recently elucidated site III contact between gp130-class cytokines and the gp130 D1 domain (*21*). However, in that interaction, the cytokine forms contacts exclusively through loops at the tip of the cytokine, rather than with residues on the helical surfaces.

In the IL-2Rα structure, the core D1 and D2 domains are separated by a 42-residue interdomain linker peptide (Thr^{65} to His^{103}), and the second domain has an additional C-terminal 54-residue connecting peptide leading to the cell membrane (Gly^{165} to Glu^{217}). Neither of these linkers is visible in the electron density

Departments of Microbiology and Immunology, and Structural Biology, Stanford University School of Medicine, 299 Campus Drive, Fairchild D319, Stanford, CA 94305–5124, USA.

*These authors contributed equally to this work.
†To whom correspondence should be addressed. E-mail: kcgarcia@stanford.edu